Exploiting $h \to W^*W^*$ decays at the upgraded Fermilab Tevatron

Tao Han
Department of Physics, University of Wisconsin, 1150 University Avenue, Madison, Wisconsin 53706

André S. Turcot
Department of Physics, University of Michigan, Ann Arbor, Michigan 48109

Ren-Jie Zhang
Department of Physics, University of Wisconsin, 1150 University Avenue, Madison, Wisconsin 53706

(Received 8 December 1998; published 18 March 1999)

We study the observability of a standard-model-like Higgs boson at an upgraded Fermilab Tevatron via the mode $h \to W^*W^*$. We concentrate on the main channel $gg \to h \to W^*W^* \to l\bar{\nu} l \nu$. We also find the mode $q\bar{q}' \to W^{\pm}h \to W^{\pm}W^*W^* \to l^{\pm}\nu l^{\pm}\nu jj$ useful. We perform detector level simulations by making use of a Monte Carlo program SHW. Optimized searching strategy and kinematical cuts are developed. We find that with a c.m. energy of 2 TeV and an integrated luminosity of 30 fb^{-1} the signal should be observable at a 3σ level or better for the mass range of 145 GeV$\lesssim m_h \lesssim$180 GeV. For 95% confidence-level exclusion, the mass reach is 135 GeV$\lesssim m_h \lesssim$190 GeV. We also present results of studying these channels with a model-independent parametrization. Further improvement is possible by including other channels. We conclude that the upgraded Fermilab Tevatron will have the potential to significantly advance our knowledge of Higgs boson physics. [S0556-2821(99)04307-6]

PACS number(s): 14.80.Bn, 13.85.Qk

I. INTRODUCTION

The mass generation mechanisms for electroweak gauge bosons and for fermions are among the most prominent mysteries in contemporary high-energy physics. In the standard model (SM) and its supersymmetric (SUSY) extensions, elementary scalar doublets of the $SU_L(2)$ interactions are responsible for the mass generation. The scalar Higgs bosons are thus crucial ingredients in the theory, and searching for the Higgs bosons has been one of the major motivations in current and future collider programs [1]. Although the masses of Higgs bosons are free parameters in the models, they are subject to generic bounds based on theoretical arguments. The triviality bound indicates that the Higgs boson mass (m_h) should be less than about 800 GeV for the SM to be a consistent low-energy effective theory [2]. A vacuum stability argument, on the other hand, suggests a correlation between the m_h lower bound and the new physics scale Λ beyond which the SM is no longer valid [3]. In other words, the discovery of a SM-like Higgs boson implies a scale Λ at which new physics beyond the SM must set in, and the smaller m_h is, the lower Λ would be. In the minimal supersymmetric standard model (MSSM), it has been shown that the mass of the lightest neutral Higgs boson must be less than about 130 GeV [4], and in any weakly coupled SUSY theory m_h should be lighter than about 150 GeV [5]. On the experimental side, the nonobservation of a Higgs signal at the CERN e^+e^- collider LEP2 experiments has established a lower bound on the SM Higgs boson mass of 89.8 GeV at a 95% confidence level (C.L.) [6]. Future searches at LEP2 will eventually be able to discover a SM Higgs boson with a mass up to 105 GeV [7]. The CERN Large Hadron Collider (LHC) is believed to be able to cover up to the full m_h range of theoretical interest, about 1000 GeV [8], although it will be challenging to discover a Higgs boson in the ''intermediate''-mass region 110 GeV$< m_h <$150 GeV, due to the huge SM background to $h \to b\bar{b}$ and the requirement of an excellent diphoton mass resolution for the $h \to \gamma\gamma$ signal.

More recently, how much the Fermilab Tevatron upgrade can do for the Higgs boson search has been intensively studied [9]. It appears that the most promising processes continuously going beyond the LEP2 reach would be the associated production of an electroweak gauge boson and the Higgs boson [10–12]:

$$p\bar{p} \to WhX, ZhX. \tag{1}$$

The leptonic decays of W,Z provide a good trigger and $h \to b\bar{b}$ may be reconstructible with adequate b tagging. It is now generally believed that for an upgraded Tevatron with a c.m. energy $\sqrt{s}=2$ TeV and an integrated luminosity $\mathcal{O}(10–30)$ fb^{-1} a SM-like Higgs boson can be observed at a $(3–5)\sigma$ level up to a mass of about 120 GeV [13]. The Higgs boson discovery through these channels crucially depends upon the b-tagging efficiency and the $b\bar{b}$ mass resolution. It is also limited by the event rate for $m_h > 120$ GeV. It may be possible to extend the mass reach to about 130 GeV by combining leptonic W,Z decays [9] and slightly beyond via the decay mode $h \to \tau^+\tau^-$ [12]. It is interesting to note that this mass reach is just near the theoretical upper bound in the MSSM. In the context of a general weakly coupled SUSY model, it would be of great theoretical significance for the upgraded Tevatron to extend the Higgs boson coverage to $m_h \sim 150$ GeV. Moreover, it would have interesting implications on our knowledge for a new physics scale Λ if we

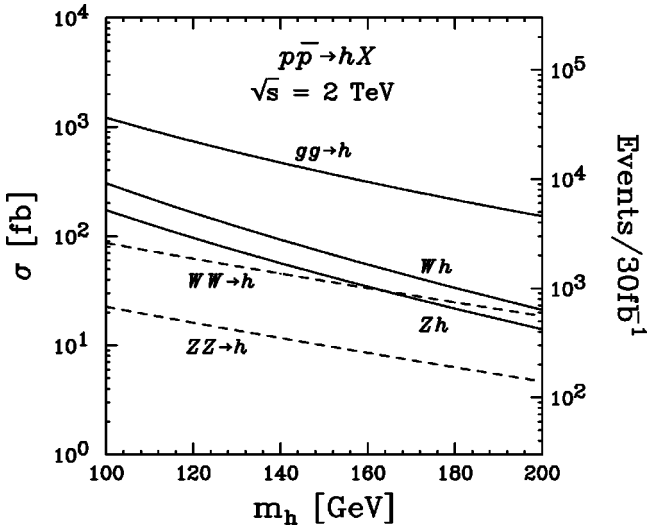

FIG. 1. The leading Higgs boson production cross sections (in fb) versus m_h at the 2 TeV Tevatron. The solid curves are for $gg\to h$, $q\bar{q}'\to W^{\pm}h$ and $q\bar{q}\to Zh$. The dashed curves are for W^+W^- and ZZ fusion to h. The scale on the right-hand side indicates the number of events per 30 fb^{-1} integrated luminosity. QCD corrections [15–17] have been included.

do find a SM-like Higgs boson or exclude its existence in the mass range 130–180 GeV, the so-called ''chimney region'' between the triviality upper bound and the vacuum stability lower bound [14].

It is important to note that the leading production mechanism for a SM-like Higgs boson at the Tevatron is the gluon-fusion process via heavy quark triangle loops:

$$p\bar{p}\to ggX\to hX. \tag{2}$$

There are also contributions to h production from the vector boson fusion processes[1]

$$W^*W^*,\ Z^*Z^*\to h, \tag{3}$$

where W^*W^* and Z^*Z^* are radiated off the quark partons. In Fig. 1, we present cross sections for SM Higgs boson production at the Fermilab Tevatron for processes (1), (2), and (3). We see that the gluon-fusion process yields the largest cross section, typically a factor of 4 above the associated production (1). For $m_h>160$ GeV, WW,ZZ fusion processes become comparable to that of Eq. (1). In calculating the total cross sections, the QCD corrections have been included for all the processes [15–17], and we have used the CTEQ4M parton distribution functions [18].

Although the decay mode $h\to b\bar{b}$ in Eqs. (2) and (3) would be swamped by the QCD background, the decay modes to vector boson pairs,

$$h\to W^*W^*, Z^*Z^*, \tag{4}$$

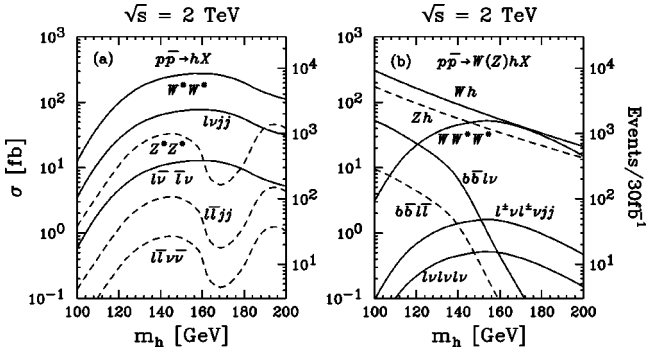

FIG. 2. The Higgs boson production cross sections (in fb) and various subsequent decay modes versus m_h at the 2 TeV Tevatron for (a) $gg\to h\to W^*W^*$ (solid curves) and Z^*Z^* (dashed curves), (b) $q\bar{q}'\to Wh$ with $h\to W^*W^*$ (solid curves) and Zh (dashed curves). Also shown are $h\to b\bar{b}$ with W,Z leptonic decays. The scales on the right-hand side indicate the number of events per 30 fb^{-1} integrated luminosity.

will have increasingly large branching fractions for $m_h \gtrsim 130$ GeV and are natural channels to consider for a heavier Higgs boson. In Fig. 2(a), we show the cross sections for $gg\to h$ with $h\to W^*W^*$ and Z^*Z^* versus m_h at $\sqrt{s}=2$ TeV. The leptonic decay channels are also separately shown by solid and dashed curves, respectively, for

$$h\to W^*W^*\to l\nu jj \quad \text{and} \quad l\bar{\nu}l\nu, \tag{5}$$

$$Z^*Z^*\to l\bar{l}jj \quad \text{and} \quad l\bar{l}\nu\bar{\nu}, \tag{6}$$

where $l=e,\mu$ and j is a quark jet. The scale on the right-hand side gives the number of events expected for 30 fb^{-1}. We see that for the m_h range of current interest, there will be about 1000 events produced for the semileptonic mode $W^*W^*\to l\nu jj$ and about 300 events for the pure leptonic mode $W^*W^*\to l\bar{\nu}l\nu$. Although the $l\nu jj$ mode has a larger production rate, the $l\bar{\nu}l\nu$ mode is cleaner in terms of the SM background contamination. The corresponding modes from Z^*Z^* are smaller by about an order of magnitude. It is natural to also consider the $h\to W^*W^*$ mode from the Wh-associated production in Eq. (1). This is shown in Fig. 2(b) by the solid curves for

$$W^{\pm}h\to l^{\pm}\nu W^*W^*\to l\nu l\nu l\nu, \tag{7}$$

$$l^{\pm}\nu l^{\pm}\nu jj. \tag{8}$$

The trilepton signal is smaller than the like-sign lepton plus jets signal by about a factor of 3 due to the difference of the W decay branching fractions to $l=e,\mu$ and to jets. For comparison, also shown in Fig. 2(b) are $Wh\to b\bar{b}l\nu$ (solid curves) and $Zh\to bbl\bar{l}$ (dashed curves) via $h\to bb$. We see that the signal rates for these channels drop dramatically for a higher m_h. Comparing the h decays in Figs. 2(a) and 2(b), it makes the gauge boson pair modes of Eq. (4) a clear choice for Higgs boson searches beyond 130 GeV.

In fact, the pure leptonic channel in Eq. (5) has been studied at SSC and LHC energies [19,20] and at a 4 TeV

[1]Here and henceforth, $W^*(Z^*)$ generically denotes a $W(Z)$ boson of either on or off mass shell.

Tevatron [11]. Despite the difficulty in reconstructing m_h from this mode due to the two missing neutrinos, the obtained results for the signal identification over substantial SM backgrounds were all encouraging. In a more recent paper [21], two of the current authors carried out a parton-level study for the W^*W^* channels of Eq. (5) for the 2 TeV Tevatron upgrade. We found that the di-lepton mode in Eq. (5) is more promising than that of $l\nu jj$ due to the much larger QCD background to the latter. While the results were encouraging, realistic simulations including detector effects were called for to draw further conclusions.

In this paper, we concentrate on the pure leptonic channel and carry out more comprehensive analyses for the signal and their SM backgrounds. We perform detector-level simulations by making use of a Monte Carlo program SHW developed for the run-II SUSY/Higgs Workshop [22,9]. We present optimized kinematic cuts which can adequately suppress the large SM backgrounds and, moreover, have been structured so as to provide a statistically robust background normalization. For the $Wh\to WW^*W^*$ channel, although the trilepton signal of Eq. (7) is rather weak, the like-sign leptons plus two jets in Eq. (8) can be useful to enhance the signal observability. For completeness, we have also included the contributions from the vector boson fusion of Eq. (3) and $W\to\tau\nu\to\nu l\nu_l$ decay mode, although they are small. We also comment on the systematic effects on the signal and background measurements which would degrade signal observability. After combining all the channels studied, we find that with a c.m. energy of 2 TeV and an integrated luminosity of 30 fb^{-1}, the signal of $h\to W^*W^*$ can be observable at a 3σ level or better for the mass range of 145 GeV $\lesssim m_h\lesssim$180 GeV. For 95% C.L. exclusion, the mass reach is 135 GeV$\lesssim m_h\lesssim$190 GeV. We thus conclude that the upgraded Fermilab Tevatron will have the potential to significantly advance our knowledge of Higgs boson physics. This provides strong motivation for a luminosity upgrade of the Fermilab Tevatron beyond the Main Injector plan.

Our signal and background Monte Carlo simulation was performed using the PYTHIA package [23] interfaced with the SHW detector simulation [22]. For pair production of resonances, e.g., WW, PYTHIA incorporates the full $2\to2\to4$ matrix elements, thereby ensuring a proper treatment of the final state angular correlations. Similarly for $h\to WW$, the angular correlations between the four final-state fermions have been taken into account. The full Z/γ^* interference is simulated for ZZ production; however, the WZ process considers only the pure Z contribution. For Higgs boson production in association with a gauge boson in Eq. (1), the associated W and Z decay angular distributions are treated properly. The production cross sections for the principal background processes were normalized to $\sigma(WW)=10.4$ pb, $\sigma(t\bar{t})=6.5$ pb, $\sigma(WZ)=3.1$ pb, and $\sigma(ZZ)=1.4$ pb.

The rest of the paper is organized as follows. In Secs. II and III, we present in detail our studies for the pure leptonic and like-sign leptons plus jets signals, respectively. In Sec. IV, we first summarize our results. We then present a study of these channels with a model-independent parametrization for the signal cross section. We conclude with a few remarks.

II. DILEPTONS PLUS MISSING TRANSVERSE ENERGY SIGNAL

For the pure leptonic channel in Eq. (5), we identify the final-state signal as two isolated opposite-sign charged leptons and large missing transverse energy. The leading SM background processes are

$$p\bar{p}\to W^+W^-\to l\bar{\nu}l\nu,\quad ZZ(\gamma^*)\to\nu\bar{\nu}l\bar{l},\quad WZ(\gamma^*)\to l\bar{\nu}l\bar{l},$$
$$p\bar{p}\to t\bar{t}\to l\bar{\nu}l\nu b\bar{b},\quad p\bar{p}\to Z(\gamma^*)\to\tau^+\tau^-\to l\bar{\nu}l\nu\nu_\tau\bar{\nu}_\tau. \tag{9}$$

We first impose basic acceptance cuts for the leptons[2]:

$$p_T(e)>10\ \text{GeV},\quad |\eta_e|<1.5,$$
$$p_T(\mu_1)>10\ \text{GeV},\quad p_T(\mu_2)>5\ \text{GeV},\quad |\eta_\mu|<1.5,$$
$$m(ll)>10\ \text{GeV},\quad \Delta R(lj)>0.4,\quad \not{E}_T>10\ \text{GeV}, \tag{10}$$

where p_T is the transverse momentum and η the pseudorapidity. The cut on the invariant mass $m(ll)$ is to remove the photon conversions and leptonic J/ψ and Υ decays. The isolation cut on $\Delta R(lj)$ removes the muon events from heavy quark (c,b) decays.[3]

At this level, the largest background comes from the Drell-Yan process for $\tau^+\tau^-$ production. However, the charged leptons in this background are very much back to back and this feature is also true, although to a lesser extent, for other background processes as well. On the other hand, as a result of the spin correlation of the Higgs boson decay products, the two charged leptons tend to move in parallel. We demonstrate this point in Figs. 3 and 4 where the distributions of the azimuthal angle in the transverse plane $[\phi(ll)]$ and the three-dimensional opening angle between the two leptons $[\theta(ll)]$ for the signal and backgrounds are shown.[4] This comparison motivates us to impose the cuts

$$\phi(ll)<160^\circ,\quad \theta(ll)<160^\circ. \tag{11}$$

The $\tau^+\tau^-$ background can be essentially eliminated with the help of the additional cuts

$$p_T(ll)>20\ \text{GeV},\quad \cos\theta_{ll-\not{E}_T}<0.5,\quad M_T(l\not{E}_T)>20\ \text{GeV}, \tag{12}$$

[2]The cuts for leptons were chosen to reflect realistic trigger considerations. It is desirable to extend the acceptance in η_l.

[3]The electron identification in the SHW simulation imposes strict isolation requirements.

[4]Since we are mainly interested in the shapes of the kinematic distributions, we present them normalized to unity with respect to the total cross section with appropriate preceding cuts.

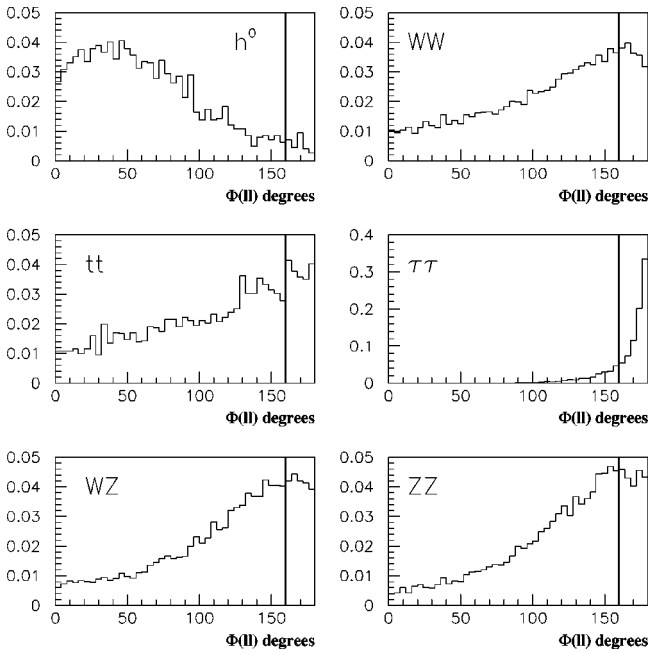

FIG. 3. Normalized azimuthal angle distributions $(1/\sigma)d\sigma/d\phi(ll)$ for the signal $gg\to h\to W^*W^*\to l\overline{\nu l}\,\nu$ with $m_h=170$ GeV and backgrounds WW, $t\overline{t}$, $\tau^+\tau^-$, WZ, and ZZ.

where $\theta_{ll-\not{E}_T}$ is the relative angle between the lepton pair transverse momentum and the missing transverse momentum, which is close to 180° for the signal and near 0° for the Drell-Yan $\tau^+\tau^-$ background. The two-body transverse mass is defined for each lepton and the missing energy as

$$M_T^2(l\not{E}_T)=2p_T(l)\not{E}_T(1-\cos\theta_{l-\not{E}_T}), \tag{13}$$

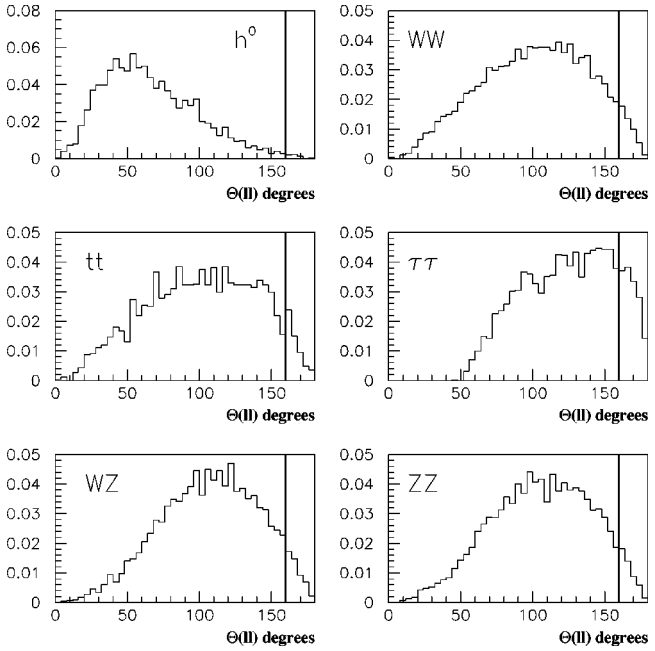

FIG. 4. Normalized distributions $(1/\sigma)d\sigma/d\theta(ll)$ for the opening angle in Eq. (11) for the signal $gg\to h\to W^*W^*\to l\overline{\nu l}\,\nu$ with $m_h=170$ GeV and backgrounds WW, $t\overline{t}$, $\tau^+\tau^-$, WZ, and ZZ.

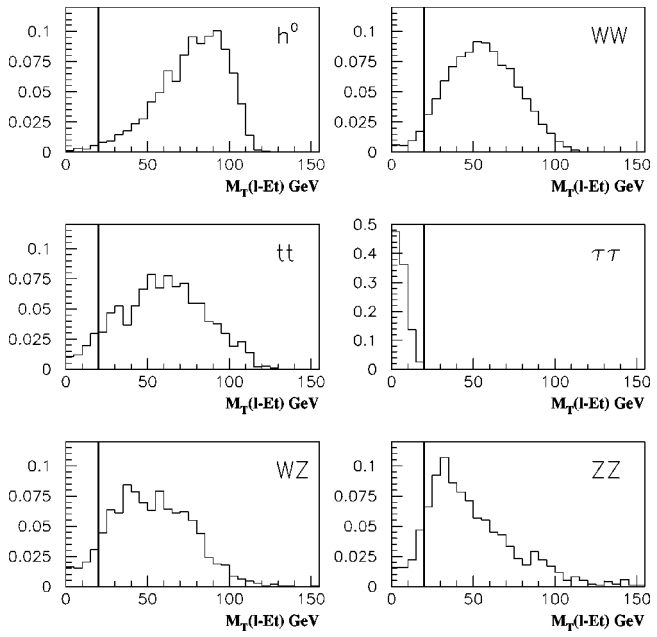

FIG. 5. Normalized distributions $(1/\sigma)d\sigma/dM_T$ for the two-body transverse mass defined in Eq. (13) for the signal $gg\to h\to W^*W^*\to l\overline{\nu l}\,\nu$ with $m_h=170$ GeV and backgrounds WW, $t\overline{t}$, $\tau^+\tau^-$, WZ, and ZZ. The minimum of $M_T(l_1\not{E}_T)$ and $M_T(l_2\not{E}_T)$ is shown.

and the distributions are shown in Fig. 5.

We can further purify the signal by removing the high $m(ll)$ events from $Z\to l\overline{l}$ as well as from $t\overline{t},W^+W^-$, as demonstrated in Fig. 6. We therefore impose

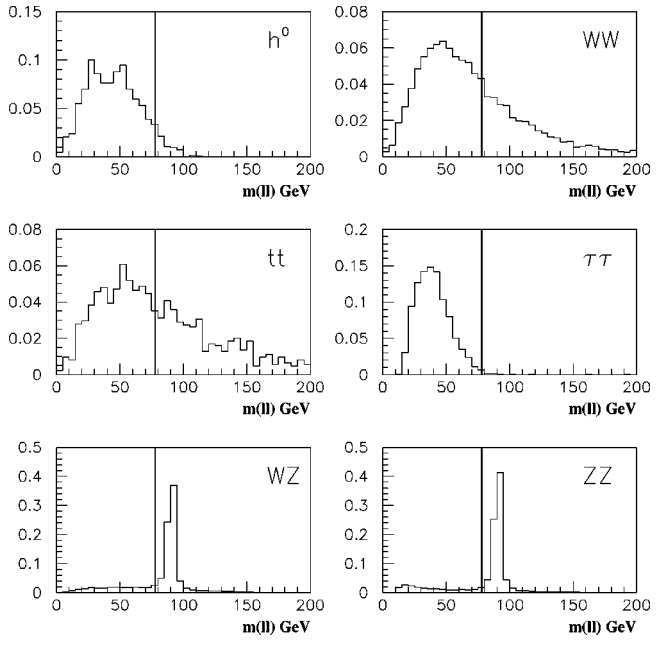

FIG. 6. Normalized like-flavor lepton-pair invariant mass distributions $(1/\sigma)d\sigma/dm(ll)$ for the signal $gg\to h\to W^*W^*\to l\overline{\nu l}\,\nu$ with $m_h=170$ GeV and backgrounds WW, $t\overline{t}$, $\tau^+\tau^-$, WZ, and ZZ.

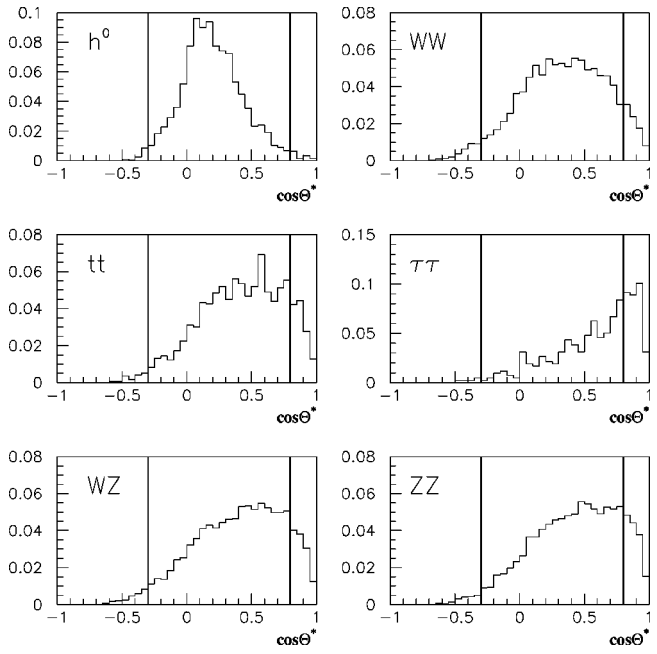

FIG. 7. Normalized distributions $(1/\sigma)d\sigma/d\cos\theta^*_{l_1}$ for the correlation angle defined above Eq. (15) for the signal $gg \to h \to W^*W^* \to l\overline{\nu l}\nu$ with $m_h = 170$ GeV and backgrounds WW, $t\bar{t}$, $\tau^+\tau^-$, WZ, and ZZ.

$$m(ll) < 78 \text{ GeV} \quad \text{for } e^+e^-, \mu^+\mu^-,$$

$$m(ll) < 110 \text{ GeV} \quad \text{for } e\mu. \tag{14}$$

As suggested in Ref. [20], the lepton correlation angle between the momentum vector of the lepton pair and the momentum of the higher p_T lepton (l_1) in the lepton-pair rest frame, $\theta^*_{l_1}$, also has discriminating power between the signal and backgrounds. This is shown in Fig. 7. We thus select events with

$$-0.3 < \cos\theta^*_{l_1} < 0.8. \tag{15}$$

A characteristic feature of the top-quark background is the presence of hard b jets. We thus devise the following jet-veto criteria[5]:

$$\text{veto if} \quad p_T^{j_1} > 95 \text{ GeV}, \quad |\eta_j| < 3,$$

$$\text{veto if} \quad p_T^{j_2} > 50 \text{ GeV}, \quad |\eta_j| < 3,$$

$$\text{veto if} \quad p_T^{j_3} > 15 \text{ GeV}, \quad |\eta_j| < 3. \tag{16}$$

[5]The previous study [21] at the parton level suggested a more stringent jet-veto cut. It turns out that it would be too costly for the signal and the more sophisticated jet-veto criterion of Eq. (16) is thus desirable.

TABLE I. $h \to W^*W^* \to l\overline{\nu l}\nu$ signal cross section (in fb) for $m_h = 140$–190 GeV and various SM backgrounds after the kinematical cuts of Eqs. (10)–(16). The signal efficiencies are also shown (in percentage). W+fake refers to the background where a jet mimics an electron with a probability of $P(j \to e) = 10^{-4}$. The backgrounds are independent of m_h.

m_h [GeV]	140	150	160	170	180	190
Signal [fb]	3.9	4.4	5.2	4.8	3.6	2.5
Efficiency [%]	35	34	38	39	36	37
	WW	$t\bar{t}$	$\tau^+\tau^-$	WZ	ZZ	W+fake
Backgrounds [fb]	130	13	0	4.4	2.4	18

Furthermore, if either of the two hard jets (j_1, j_2) is identified as a b quark, the event will be also vetoed. The b-tagging efficiency is taken to be [22]

$$\epsilon_b = 1.1 \times 57\% \ \tanh\left(\frac{\eta_b}{36.05}\right), \tag{17}$$

where the factor 1.1 reflects the 10% improvement for a lepton impact parameter tag.

The results up to this stage are summarized in Table I for the signal $m_h = 140$–190 GeV as well as the SM backgrounds. The acceptance cuts discussed above are fairly efficient, approximately 35% in retaining the signal while suppressing the backgrounds substantially. We see that the dominant background comes from the electroweak WW production, about a factor of 30 higher than the signal rate. The subleading backgrounds $t\bar{t}$ and W+fake [the background where a jet mimics an electron with a probability of $P(j \to e) = 10^{-4}$ [24]] are also bigger than the signal. We note that although the b-jet veto is effective against the $t\bar{t}$ background, the final results are not affected if the veto efficiency is significantly worse.

One can improve the signal observability by constructing a likelihood based on some characteristic kinematical variables. We choose the variables as (1) $\cos\theta_{ll}$, the polar angle with respect to the beam axis of the dilepton [20], (2) $\phi(ll)$ as in Eq. (11), (3) $\theta(ll)$ as in Eq. (11), (4) $\cos\theta_{ll-\not{E}_T}$ as in Eq. (12), (5) p_T^{j1} as in Eq. (16), and (6) p_T^{j2} as in Eq. (16). We wish to evaluate the likelihood for a candidate event to be consistent with one of five event classes: a Higgs boson signal ($140 < m_h < 190$ GeV), WW, $t\bar{t}$, WZ, or ZZ. For a single variable x_i, the probability for an event to belong to class j is given by

$$P_i^j(x_i) = \frac{f_i^j(x_i)}{\sum_{k=1}^{5} f_i^k(x_i)}, \tag{18}$$

where f_i^j denotes the probability density for class j and variable i. The likelihood of an event to belong to class j is given by the normalized products of the individual $P_i^j(x_i)$ for the $n = 6$ kinematical variables:

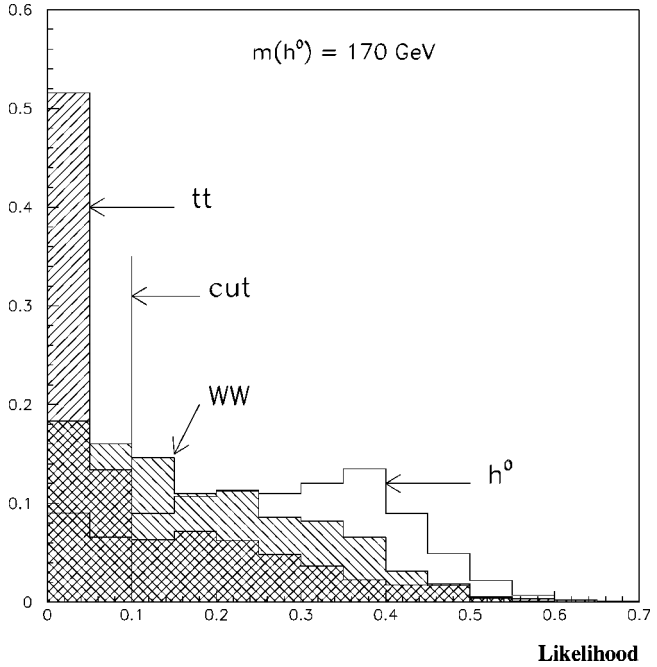

FIG. 8. Distributions for the likelihood variable defined in Eq. (19) for the signal $m_h=170$ GeV and the leading SM backgrounds WW and $t\bar{t}$.

$$\mathcal{L}^j=\frac{\Pi_{i=1}^{n}\ P_i^j(x_i)}{\Sigma_{k=1}^{5}\ \Pi_{i=1}^{n}\ P_i^k(x_i)}. \tag{19}$$

The value of $\mathcal{L}^j$ for a Higgs boson signal hypothesis ($j=1$) is shown in Fig. 8 where it can be seen that a substantial fraction of the $t\bar{t}$ and WW background can be removed for a modest loss of acceptance. The WZ and ZZ backgrounds have similar distributions to the WW and have been omitted for clarity. We thus impose the requirement

$$\mathcal{L}^{j=1}>0.10. \tag{20}$$

The improved results are summarized in Table II.

In identifying the signal events, it is crucial to reconstruct the mass peak of m_h. Unfortunately, the W^*W^* mass from the h decay cannot be accurately reconstructed due to the two undetectable neutrinos. However, both the transverse mass M_T and the cluster transverse mass M_C [25], defined as

TABLE II. $h\to W^*W^*\to l\bar{\nu}l\nu$ signal cross section (in fb) for $m_h=140$–190 GeV and various SM backgrounds after the kinematical cuts of Eqs. (10)–(16) and the likelihood cut Eq. (20). W + fake refers to the background where a jet mimics an electron with a probability of $P(j\to e)=10^{-4}$. The backgrounds are independent of m_h.

m_h [GeV]	140	150	160	170	180	190
Signal [fb]	3.1	3.6	4.5	4.1	2.9	2.0
	WW	$t\bar{t}$	$\tau^+\tau^-$	WZ	ZZ	W+fake
Backgrounds [fb]	83	4.5	0	3.1	1.8	13

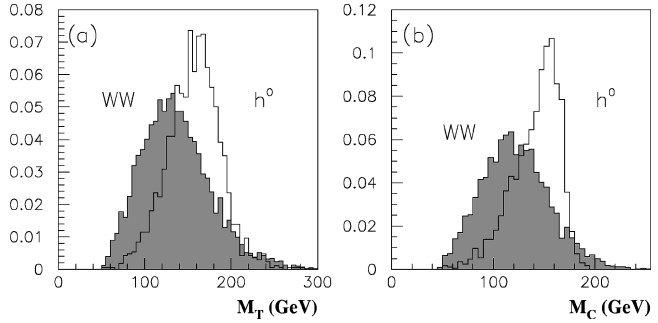

FIG. 9. Normalized distributions $(1/\sigma)d\sigma/dM$ for the signal $gg\to h\to W^*W^*\to l\bar{\nu}l\nu$ with $m_h=170$ GeV (histogram) and the leading WW background (shaded) for (a) the transverse mass defined in Eq. (21) and (b) the cluster transverse mass defined in Eq. (22).

$$M_T=2\sqrt{p_T^2(ll)+m^2(ll)}, \tag{21}$$

$$M_C=\sqrt{p_T^2(ll)+m^2(ll)}+\not{E}_T, \tag{22}$$

yield a broad peak near m_h and have a long tail below. The cluster transverse mass M_C has a Jacobian structure with a well-defined edge at m_h. We show the nature of these two variables for the signal with $m_h=170$ GeV and the leading WW background in Fig. 9(a) for M_T and (b) for M_C after application of the likelihood cut. For a given m_h to be studied, one can perform additional cut optimization. In Table III, we list m_h-dependent criteria for the signal region defined as

$$m_h-60<M_C<m_h+5\ \text{GeV}. \tag{23}$$

We illustrate the effect of the optimized cuts of Table III in Fig. 10, where the cluster tranverse mass distribution for a $m_h=170$ GeV signal and the summed backgrounds, normalized to 30 fb^{-1}, are shown before (a) and after (b) the final cuts. A clear excess of events from the Higgs signal can be seen in Fig. 10(b). It is important to note that before application of the final cuts, the dominant backgrounds are WW and the W+fake with other sources accounting for less than 10% of the total. Moreover, for 30 fb^{-1} integrated luminosity, the statistical error in the background is less than 2% before application of the final cuts. We therefore argue that

TABLE III. Summary of the optimized cuts additional to those in Eqs. (10)–(16) for various Higgs boson mass.

m_h [GeV]	140	150	160	170	180	190
$\cos\theta^*_{l_1}$		<0.6	0.35	0.35	0.55	0.75
$\not{E}_T$	>25	25	30	35	40	40
$\min[M_T(l_1\not{E}_T),M_T(l_2\not{E}_T)]$	>40	40	75	80	85	75
$M_T(l_1\not{E}_T)$	>60	60				
$m(ll)$	<65	65	65	75	85	
$p_T(ll)$	>40	50	65	70	70	70
$\theta(ll)$	<100	100	70	70	90	90
M_T		>110	120	130	140	140

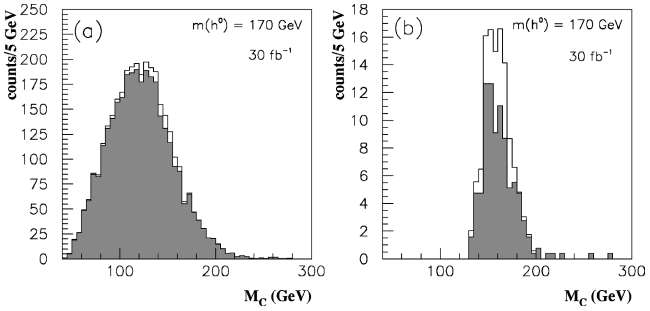

FIG. 10. Cluster transverse mass distributions for the leading WW background (shaded) and the background plus the signal $gg\to h\to W^*W^*\to l\overline{\nu l}\nu$ with $m_h=170$ GeV (histogram) (a) before the optimized cuts in Table III and (b) after the cuts. The vertical axis gives the number of events per 5 GeV bin for 30 fb^{-1}.

one should be able to normalize the SM background curve (WW) with sufficient precision to unambiguously identify a significant excess attributable to a Higgs boson signal. It should also be noted that by selectively loosening the final cuts, it is possible to maintain the same $S/\sqrt{B}$ while increasing the accepted background by up to factor of 5, and the accepted signal by a factor of 2.5. This can provide a powerful cross-check of the predicted background M_C shape and can be used to demonstrate the stability of any observed excess.

Our final results for the channel $h\to W^*W^*\to l\overline{\nu l}\nu$ are summarized in Table IV. We have included the contributions to $h\to W^*W^*$ from the signal channels in Eqs. (1) and (3). Although they are small to begin with, they actually increase the accepted signal cross section by (12–18) %. We have also included the contribution from $W\to\tau\nu\to l\nu_l\nu$.[6] It can be seen that one may achieve a S/B of at least 6% for 140 GeV$<m_h<$190 GeV and reach 45% for $m_h=170$ GeV. The statistical significance, $S/\sqrt{B}$, for 30 fb^{-1} integrated luminosity, is 3σ or better for $150<m_h<180$ GeV. In Fig. 11(a), we present the integrated luminosities needed to reach a 3σ significance and 95% C.L. exclusion computed assuming Poisson probabilities for m_h.

To assess the effect of inherent systematic uncertainties, we reevaluate the corresponding curves in Fig. 11(b) assuming a 10% systematic error for the signal and SM backgrounds.[7] The results are somewhat degraded, but they are still encouraging.

III. LIKE-SIGN DILEPTON PLUS JETS SIGNAL

When considering the $h\to W^*W^*$ mode in the associated production channels of Eq. (1), it is natural to consider the trilepton mode of Eq. (7) [26]. However, the leptonic branching fractions for the W decays limit the signal rate. Also, the leading irreducible SM background $WZ(\gamma^*)\to 3l$ is difficult to suppress to a sufficient level. On the other hand, the $W^*W^*\to l\nu jj$ mode gives like-sign leptons plus two-jets events [10,26] as in Eq. (8) with a 3 times larger rate than the trilepton mode, while the leading background is higher order than $WZ(\gamma^*)$. In this case, the contributing channels include

$$Wh\to WW^*W^*\to l^\pm\nu l^\pm\nu jj,$$

$$Wh\to WZ^*Z^*\to l^\pm\nu l^\pm l^\mp jj,$$

$$Zh\to ZW^*W^*\to l^\pm l^\mp l^\pm\nu jj,$$

$$Zh\to ZZ^*Z^*\to l^\pm l^\mp l^\pm l^\mp jj.$$

We identify the final state signal as two isolated like-sign charged leptons plus jets. A soft third lepton may be present. The SM backgrounds are

$$p\overline{p}\to WWW, WWZ, WZZ, ZZZ, t\overline{t}W, t\overline{t}Z\to l^\pm l^\pm jjX, \tag{24}$$

TABLE IV. Summary table for $h\to W^*W^*\to l\overline{\nu l}\nu$ signal for $m_h=140$–190 GeV and various SM backgrounds after the kinematical cuts of Eqs. (10)–(16) and the likelihood cut Eq. (20). W + fake refers to the background where a jet mimics an electron with a probability of $P(j\to e)=10^{-4}$. The backgrounds are independent of m_h.

m_h [GeV]	140	150	160	170	180	190
$gg\to h$ [fb]	2.2	2.4	1.3	0.93	0.85	0.73
Associated VH [fb]	0.26	0.31	0.13	0.09	0.06	0.06
VV fusion [fb]	0.12	0.12	0.09	0.06	0.05	0.05
Signal sum [fb]	2.6	2.8	1.5	1.1	0.96	0.83
SM backgrounds [fb]	39	27	4.1	2.3	3.8	7.0
Fake $j\to e$ [fb]	5.1	3.4	0.34	0.15	0.08	0.45
Backgrounds sum [fb]	44	30	4.4	2.4	3.8	7.5
S/B [%]	5.8	9.4	34	45	25	11
$S/\sqrt{B}$ [30 fb^{-1}]	2.1	2.8	3.9	3.8	2.7	1.7

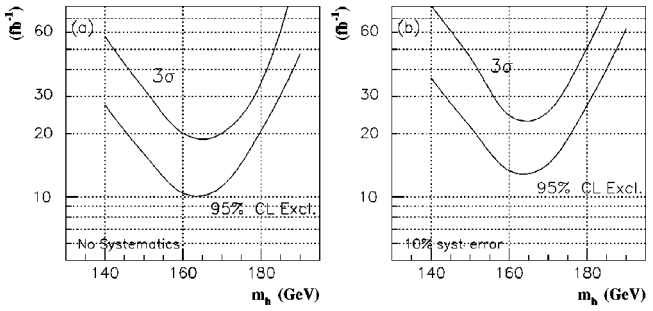

FIG. 11. The integrated luminosity required to reach 3σ statistical significance and 95% exclusion versus m_h in the $h\to W^*W^*\to l\overline{\nu l}\nu$ channel for (a) statistical effects only and (b) 10% systematic error for the signal and SM backgrounds included. The contributions from $W\to\tau\to l$ decays, associated production, and gauge boson fusion have also been included.

[6]From consideration of the $W+(j\to e)$ background, it should be clear that improving the sensitivity by incorporating hadronic tau decays will be a difficult task. We nonetheless encourage the effort.

[7]For the purposes of computing the effects of systematic errors on the sensitivity to a Higgs signal, we have scaled the expected background upward by a given percentage and the expected signal downward by the same percentage simultaneously.

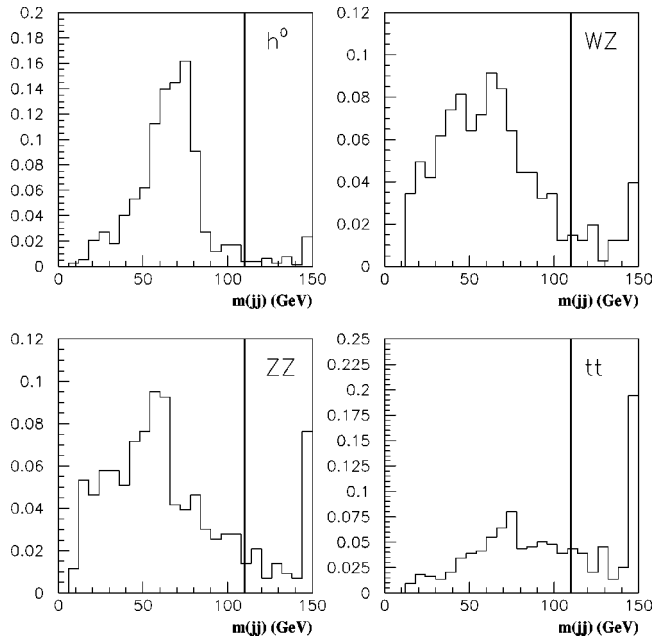

FIG. 12. Normalized dijet mass distributions $(1/\sigma)d\sigma/dm(jj)$ for the signal $W^{\pm}h\to W^{\pm}W^{*}W^{*}\to l^{\pm}l^{\pm}jj$ with $m_h=170$ GeV and the backgrounds WZ, ZZ, and $t\bar{t}$.

$$p\bar{p}\to W^{\pm}Z(\gamma^{*})+jj\to l^{\pm}l^{\pm}jjX,$$

$$ZZ(\gamma^{*})+jj\to l^{\pm}l^{\pm}jjX,\quad t\bar{t}\to l\bar{\nu}jjb\bar{b}, \tag{25}$$

$$p\bar{p}\to Wjj,\ Z(\gamma^{*})jj+\text{fake}.$$

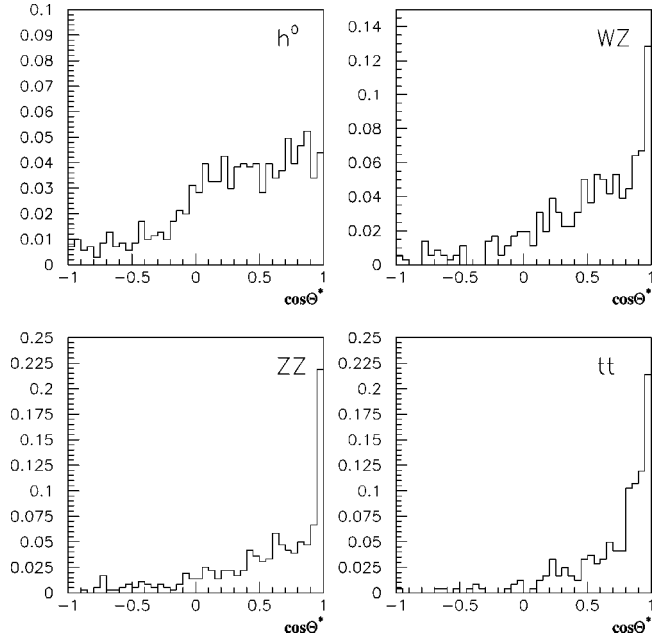

FIG. 13. Normalized distributions $(1/\sigma)d\sigma/d\cos\theta_{l_1}^{*}$ for the correlation angle defined above Eq. (15) for the signal $W^{\pm}h\to W^{\pm}W^{*}W^{*}\to l^{\pm}l^{\pm}jj$ with $m_h=170$ GeV and backgrounds WZ, ZZ, and $t\bar{t}$.

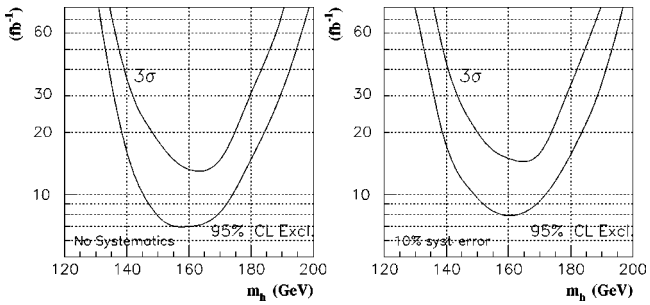

FIG. 14. The integrated luminosity required to reach 3σ statistical significance and 95% C.L. exclusion versus m_h in combining both channels $h\to W^{*}W^{*}\to l\bar{\nu}l\nu$ and $W^{\pm}h\to W^{*}W^{*},Z^{*}Z^{*}\to l^{\pm}l^{\pm}jj$ for (a) statistical effects only and (b) 10% systematic error included for these two channels.

Although the triple gauge boson production [27] in Eq. (24) constitutes the irreducible backgrounds, the $WZjj,t\bar{t}$ through b or c semileptonic decay and the background from $j\to e$ fakes turn out to be larger.

The basic acceptance cuts required for the leptons are

$$p_T(l)>10\ \text{GeV},\quad |\eta_l|<1.5,\quad m(ll)>10\ \text{GeV},$$

$$0.3<\Delta R(lj)<6,\quad \not{E}_T>10\ \text{GeV}. \tag{26}$$

For a muon, we further demand that the scalar sum of additional track momenta within 30° be less than 60% of the muon momentum. We require that there be at least two jets with

$$p_T^{j}>15\ \text{GeV},\quad |\eta_j|<3. \tag{27}$$

To suppress the WZ background, we require the leading jet to be within $|\eta_{j_1}|<1.5$ and to have a charged track multiplicity satisfying $2\leqslant N\leqslant 12$, while the subleading jet to be within $|\eta_{j_2}|<2.0$. The $t\bar{t}$ background typically exhibits greater jet activity; we therefore veto events having

$$p_T^{j_3}>30\ \text{GeV}, \tag{28}$$

and events with a fourth jet satisfying Eq. (27). To suppress backgrounds associated with heavy flavor jets, we veto the event if any of the jets have a b tag.

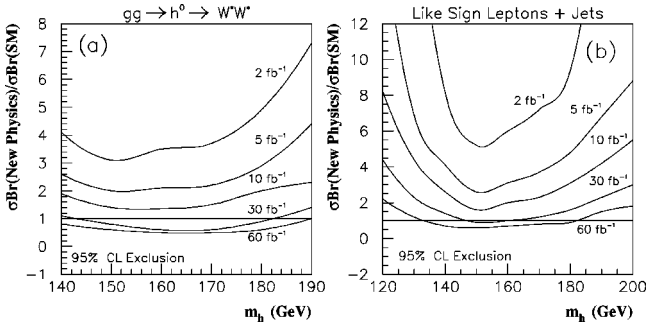

FIG. 15. 95% C.L. exclusion for the ratio R [Eq. (33)] versus m_h for several values of the integrated luminosity (a) for the channel Eq. (31) and (b) for Eq. (32).

TABLE V. $Vh \to l^{\pm}l^{\pm}jj$ signal for $m_h = 120$–200 GeV and the SM backgrounds after the kinematical cuts of Eqs. (26)–(29).

m_h [GeV]	120	130	140	150	160	170	180	190	200
Signal sum [fb]	0.093	0.20	0.34	0.52	0.45	0.38	0.29	0.20	0.16
Background channels	WZ	ZZ	WW	$t\bar{t}$	VVV	$t\bar{t}V$	$W/Z\ jj$ + fake	Sum	
σ [fb]	0.27	0.06	0.01	0.15	0.07	0.02	0.26 [31]	0.83	
S/B [%]	11	24	41	63	54	46	35	24	19
$S/\sqrt{B}$ [30 fb^{-1}]	0.56	1.2	2.0	3.1	2.7	2.3	1.7	1.3	0.96

In Fig. 12, we present the dijet mass distributions for the signal and backgrounds. Since the dijets in the signal are mainly from a W^* decay, $m(jj)$ is close to or lower than M_W. This motivates us to further require

$$m(jj) < 110 \text{ GeV}, \quad \Sigma_j |p_T^j| < 150 \text{ GeV}. \tag{29}$$

Finally, it is interesting to note that the lepton correlation angle introduced in Eq. (15) has strong discriminating power to separate the signal from backgrounds as shown in Fig. 13. We then impose a final cut

$$\cos\theta_{l_1}^* < 0.95. \tag{30}$$

With these cuts, we present the results for the signal and backgrounds in Table V. We can see that for a given m_h, the S/B is larger than that for the dilepton plus $\not{E}_T$ signature, reaching as high as 63%. One can consider further optimization of cuts with m_h dependence. However, the rather small signal rate for a 30 fb^{-1} luminosity limits the statistical significance. Also, the systematic uncertainty in the background may be worse than the purely leptonic channel.

IV. DISCUSSIONS AND CONCLUSION

We have carried out comprehensive studies for $h \to W^*W^*$ via the two channels

$$p\bar{p} \to h \to W^*W^* \to l\bar{\nu} l \nu, \tag{31}$$

$$p\bar{p} \to W^{\pm}h, \ Zh \to W^{\pm}(Z)W^*W^* \to l^{\pm}l^{\pm}jj. \tag{32}$$

In combining both channels, we present our summary figure in Fig. 14, again for (a) statistical effects only and (b) 10% systematic error for the signal and SM backgrounds included for both channels. We conclude that with a c.m. energy of 2 TeV and an integrated luminosity of 30 fb^{-1} the Higgs boson signal via $h \to W^*W^*$ should be observable at a 3σ level or better for the mass range of 145 GeV$\lesssim m_h \lesssim$180 GeV. For 95% C.L. exclusion, the mass reach is 135 GeV$\lesssim m_h \lesssim$190 GeV.

Our results presented here are valid not only for the SM Higgs boson, but also for SM-like ones such as the lightest supersymmetric Higgs boson in the decoupling limit [28]. A Higgs mass bound can be translated into exploring fundamental parameters for a given theoretical model, as shown in Ref. [29]. Furthermore, if there is an enhancement for $\Gamma(h \to gg) \times \mathcal{B}(h \to WW, ZZ)$ over the SM expectation, or if $\mathcal{B}(h \to b\bar{b})$ is suppressed, such as in certain parameter region in SUSY [30], the signals of Eq. (4) would be more substantial and more valuable to study. We can make our study more general in this regard by considering the quantity $\sigma(h) \times \mathcal{B}(h \to W^*W^*)$ as a free parameter. Define a ratio of this parameter to the SM expectation for the signal to be

$$R = \frac{\sigma(h) \times \mathcal{B}(h \to W^*W^*)_{new\ physics}}{\sigma(h) \times \mathcal{B}(h \to W^*W^*)_{SM}}. \tag{33}$$

Measuring R would represent a generic Higgs boson search in a model-independent way. Figure 15 gives the 95% C.L. exclusion for the ratio R versus m_h for several values of the integrated luminosity, where $R=1$ corresponds to the SM expectation. Figure 15(a) is for the channel Eq. (31), where we have only included the gluon-fusion contribution, and Fig. 15(b) for Eq. (32). On the other hand, once a Higgs boson signal is established, a careful examination of R would help confirm the SM or identify possible new physics.

Finally, we would like to point out that further improvement on our results is still possible by including other channels. Although there would be even larger SM backgrounds, the channel $h \to W^*W^* \to l\nu jj$ was found [21] to be helpful in improving the Higgs boson coverage. Combining with $h \to Z^*Z^* \to lljj$ as shown in Fig. 2, we would expect some possible improvement which deserves further study. The channels $h \to Z^*Z^* \to l\bar{l}\nu\bar{\nu}, 4l$ may have smaller SM backgrounds, especially for the $4l$ mode. Unfortunately, the signal rate would be very low for the anticipated luminosity at the Tevatron. It is nevertheless prudent to keep them in mind in searching for the difficult Higgs boson signal.

In summary, we have demonstrated the feasibility for an upgraded Tevatron to significantly extend the Higgs boson mass coverage. The Fermilab Tevatron with a luminosity upgrade will have the potential to significantly advance our knowledge of Higgs boson physics.

ACKNOWLEDGMENTS

We would like to thank the participants of the Tevatron run-II Higgs Working Group, especially M. Carena, J. Conway, H. Haber, J. Hobbs, J.-M. Qian, D. Rainwater, S. Willenbrock, and D. Zeppenfeld for discussions. We would also like to thank T. Junk for making available the programs used to calculate the sensitivity in the Poissonian limit and E. Flattum for developing the SHW/PAW interface. This work was supported in part by DOE Grant No. DE-FG02-95ER40896 and in part by the Wisconsin Alumni Research Foundation. A.S.T. acknowledges the support from the University of Michigan by DOE Grant No. DE-FG02-95ER40899.

[1] J. Gunion, H. Haber, G. L. Kane, and S. Dawson, *The Higgs Hunter's Guide* (Addison-Wesley, Redwood City, CA, 1990); *Perspectives on Higgs Physics II*, edited by G. L. Kane (World Scientific, Singapore, 1997).

[2] U. M. Heller, M. Klomfass, H. Neuberger, and P. Vranas, Nucl. Phys. **B405**, 555 (1993), and references therein.

[3] G. Altarelli and G. Isidori, Phys. Lett. B **337**, 141 (1994); J. A. Casas, J. R. Espinosa, and M. Quiros, *ibid.* **342**, 171 (1995); **382**, 374 (1996).

[4] H. Haber and R. Hempfling, Phys. Rev. D **48**, 4280 (1993); R. Hempfling and A. H. Hoang, Phys. Lett. B **331**, 99 (1994); M. Carena, J. R. Espinosa, M. Quiros, and C. E. M. Wagner, *ibid.* **355**, 209 (1995); M. Carena, M. Quiros, and C. E. M. Wagner, Nucl. Phys. **B461**, 407 (1996); H. Haber, R. Hempfling, and A. H. Hoang, Z. Phys. C **75**, 539 (1997).

[5] G. L. Kane, C. Kolda, and J. D. Wells, Phys. Rev. Lett. **70**, 2686 (1993).

[6] D. Treille, presented at the XXIX International Conference on High Energy Physics, Vancouver, Canada, 1998, and reference therein.

[7] For a recent review on Higgs boson physics at LEP2, see, e.g., M. Carena *et al.*, in *Physics at LEP2* (CERN Report No. 96-01, Geneva, 1996), p. 351, hep-ph/9602250.

[8] CMS Technical Design Report No. CERN-LHCC-94-38; ATLAS Technical Design Report No. CERN-LHCC-94-43.

[9] For more information, visit the homepage of the Higgs Working Group for Tevatron Run-II at http://fnth37.fnal.gov/higgs.html, and references therein.

[10] A. Stange, W. Marciano, and S. Willenbrock, Phys. Rev. D **49**, 1354 (1994); **50**, 4491 (1994); A. Belyaev, E. Boos, and L. Dudko, Mod. Phys. Lett. A **10**, 25 (1995).

[11] J. Gunion and T. Han, Phys. Rev. D **51**, 1051 (1995).

[12] S. Mrenna and G. L. Kane, hep-ph/9406337.

[13] S. Kim, S. Kuhlmann, and W. M. Yao, in Proceedings of 1996 DPF/DPB Summer Study on ''New Directions for High-energy Physics,'' Snowmass, 1996, p. 610; W. M. Yao, *ibid.*, p. 619.

[14] T. Hambye and K. Riesselmann, Phys. Rev. D **55**, 7255 (1997); K. Riesselmann, hep-ph/9711456, and references therein.

[15] D. Graudenz, M. Spira, and P. M. Zerwas, Phys. Rev. Lett. **70**, 1372 (1993); M. Spira, A. Djouadi, D. Graudenz, and P. M. Zerwas, Nucl. Phys. **B453**, 17 (1995).

[16] T. Han and S. Willenbrock, Phys. Lett. B **273**, 167 (1991).

[17] T. Han, G. Valencia, and S. Willenbrock, Phys. Rev. Lett. **69**, 3274 (1992).

[18] CTEQ Collaboration, H. L. Lai *et al.*, Phys. Rev. D **55**, 1280 (1997).

[19] E. W. N. Glover, J. Ohnemus, and S. S. D. Willenbrock, Phys. Rev. D **37**, 3193 (1988); V. Barger, G. Bhattacharya, T. Han, and B. A. Kniehl, *ibid.* **43**, 779 (1991).

[20] M. Dittmar and H. Dreiner, Phys. Rev. D **55**, 167 (1997).

[21] T. Han and R.-J. Zhang, Phys. Rev. Lett. **82**, 25 (1999).

[22] J. Conway, computer code SHW2.0, available at http://www.physics.rutgers.edu/~jconway/soft/shw/shw.html (unpublished).

[23] T. Sjostrand, Comput. Phys. Commun. **82**, 74 (1994); the version employed was PYTHIA 6.023.

[24] S. Abachi *et al.*, Phys. Rev. D **52**, 4877 (1995).

[25] V. Barger, T. Han, and J. Ohnemus, Phys. Rev. D **37**, 1174 (1988).

[26] H. Baer and J. D. Wells, Phys. Rev. D **57**, 4446 (1998).

[27] T. Han and R. Sobey, Phys. Rev. D **52**, 6302 (1995).

[28] H. E. Haber and Y. Nir, Nucl. Phys. **B335**, 363 (1990); H. E. Haber, in *Proceedings of the Fourth International Conference on Physics Beyond the Standard Model*, Granlibakken, Lake Tahoe, CA, 1994, edited by J. F. Gunion, T. Han and J. Ohnemus (World Scientific, Singapore, 1995), p. 151.

[29] H. Baer, B. W. Harris, and X. Tata, Phys. Rev. D **59**, 015003 (1999).

[30] M. Carena, S. Mrenna, and C. Wagner, hep-ph/9808312.

[31] The $W+3$ jet rate was taken from D0 run-I data. See, e.g., E. W. Varnes, Ph.D. thesis, Report No. LBNL-40283, UC-414, 1997.